Multi-Target Reflection Point Model of Cyclists for Automotive Radar

Martin Stolz [#], Eugen Schubert [#], Frank Meinl [#], Martin Kunert [#], Wolfgang Menzel [*]

[#]*Advanced Engineering Sensor Systems, Robert Bosch GmbH*
P.O. Box 16 61, 71226 Leonberg, Germany
martin.stolz2@de.bosch.com

[*]*Institute of Microwave Techniques, Ulm University*
Albert-Einstein-Allee 41, 89081 Ulm, Germany

***Abstract*— Pushed by the EuroNCAP regulations the number of autonomous emergency braking systems for pedestrians (AEB-P) is rapidly increasing since the year 2016. The same rise is expected for cyclist protection systems driven by new test scenarios of EuroNCAP from 2018 onwards. To get an adequate reaction of the system, target objects have to be classified clearly. Visual sensors provide some benefits in object recognition, but the performance suffers in adverse environmental conditions. In this area radar sensors have proven as very robust against darkness, fog, or rain. For classification unique features are required. To extract relevant features, a motion analysis of cyclists is presented in this work which is subsequently used to derive a reflection point model. Specific properties of radar evaluation have been added to the model too. In combination with an automotive radar sensor model, detection limits of actual sensors can be explored. It is also possible to determine the performance requirements for future sensor generations and to evaluate new signal processing algorithms.**

I. Introduction

The demand of advanced driver assistant systems (ADAS) for vulnerable road user increased during the last few years. Primarily forced by the ratings of EuroNCAP active pedestrian safety systems like automatic emergency braking for pedestrians (AEB-P) are increasingly implemented. According to the roadmap of EuroNCAP from 2018, also AEB systems for cyclists will be rated. An appropriate sensor technology is an automotive radar which often builds the basis for this functions. The ability to measure distance, speed and angle in high-resolution with a single measurement snapshot on the one hand and the insensitivity against environmental conditions like fog, rain and bad visibility at night on the other hand are the big advantages.

Automotive radar sensors are also used in the domain of highly automated driving for environmental perception. Therefore it is required to differentiate between the diverse road users and react in an adequate manner. To classify detected targets, significant features of every road user have to be extracted from the signals.

Prior research on feature extraction based on automotive radar for pedestrians is shown in [1], [2]. To extract features, the well-known model of motion from a pedestrian is used. The different velocities of moving limbs result in a spread of the velocity from zero to three-times the bulk motion of pedestrians. With a high-resolution automotive radar on the basis of μ-doppler effects [3] the velocity spread is measurable.

To extract significant features for cyclists, a model near to reality and focused on automotive radar capabilities is useful. Known modelling of bicycles [4] refers to the movement dynamics of the entire bicycle system like self-stabilization and gyroscopic effects. The velocity spread of a bicycle as shown in [1] is not taken into account.

The new model must provide accurate details of velocity and distance. For the distance, an illustration of the frame geometry respectively of the entire bicycle is necessary. To get velocities of the parts of a cyclist, detailed analysis of the motion is required where a model as simple as possible and close to reality is preferred.

The model can also be used as a basis for the development of new functions and algorithms. In this context, the possibility to generate reproducible scenarios for the evaluation of the performance of algorithms is of great importance. In the present case, the model is applied in the development of algorithms for the classification of cyclists.

The first part of this paper investigates in the movement of a cyclist. Body and bicycle parts with their different velocities are discussed in detail. We continue with the description of the simulated model based on reflection points. In the last part, first results of simulation data are shown in a three dimensional detection point cloud and in the range-velocity spectrum. Comparison of the simulation data with real measurement data completes the execution.

II. Movement Analysis

The system cyclist consists of two main parts: rider and bicycle. In order to accelerate a bicycle, the pedal movement of the legs is converted into a rotating movement of the wheels. Thereby different individual periodic processes are accomplished during one pedal rotation. Without limitation of generality it is assumed, that only the pedals, legs and wheels perform a movement different from the given uniform movement speed $\vec{v}_{ego}$, as described below.

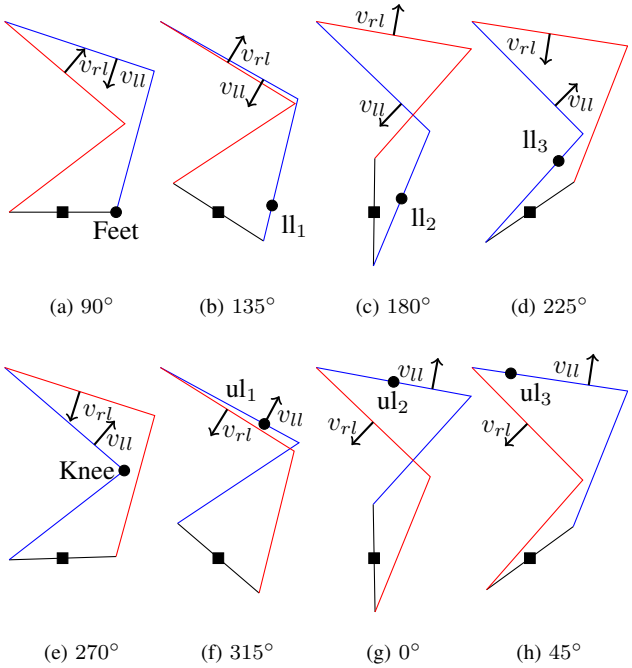

Fig. 1. Movement of legs for one pedal rotation (—) right leg, (—) left leg and (—) pedal with approximated points

A. Pedal Movement

The pedals perform a uniform circular rotation $\vec{\omega}_p$ around the bottom bracket with distance $\vec{r}(t)$ determined by the pedal crank length. Considering that the ego motion $\vec{v}_{ego}$ is added to the pedal speed, it results in a oscillating speed $\vec{v}_p(t)$ over time around the movement speed for one pedal rotation.

$$\begin{aligned} \vec{v}_{t,p}(t) &= \vec{\omega}_p \times \vec{r}(t) \\ \vec{v}_p(t) &= \vec{v}_{t,p}(t) + \vec{v}_{ego} \end{aligned} \tag{1}$$

B. Leg Movement

Different types of movement are observable with respect to the legs. To describe them in detail, the leg is divided into three parts: foot, upper and lower leg.

1) foot: Depending on the pedal speed, a complete circular movement superimposed with the ego motion is recognizable on the feet with the defined $\vec{v}_p(t)$ pedal speed.

2) upper leg: Upper leg rotates around the hip $\vec{\omega}_h(t)$ in clockwise and counter clockwise direction with a non uniform movement in a limited angular range with $\vec{v}_{t,ul}(t)$ dependent on the length $\vec{r}(t)$ of the upper leg. Upper leg speed $\vec{v}_{ul}(t)$ is superimposed with the movement speed $\vec{v}_{ego}$ of the cyclist and results to

$$\begin{aligned} \vec{v}_{t,ul}(t) &= \vec{\omega}_h(t) \times \vec{r}(t) \\ \vec{v}_{ul}(t) &= \vec{v}_{t,ul}(t) + \vec{v}_{ego} \end{aligned} \tag{2}$$

3) lower leg: The movement of the lower leg is a combination of the continuous movement of the feet, the non linear agitation of the knee and the non uniform rotation motion of the lower leg, which is approximated numerically.

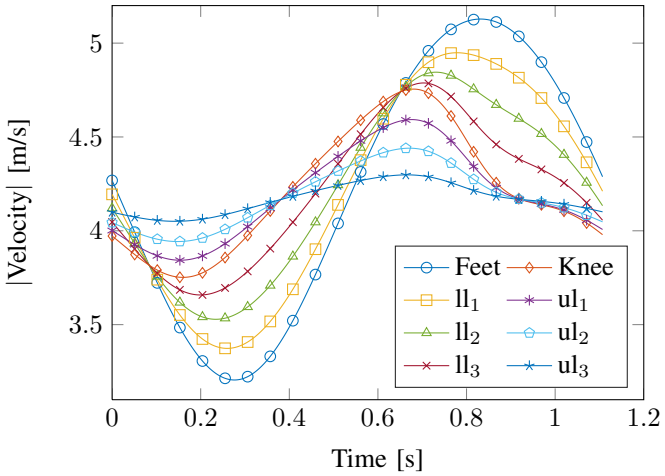

Fig. 2. Example of a velocity profile for approximated points on the legs

In Fig. 1 one pedal rotation of the legs is indicated. The velocity vectors without the ego motion are also drawn. For the cyclist model the legs are approximated by points whose positions are additionally indicated in the figure. The resulting speed profile of the approximated points on the legs for one pedal rotation is drawn in Fig. 2 with reference to the motion equations. The oscillating speed of the legs around the uniform movement is easy to identify. The magnitude of the oscillating speed depends on the distance of the point from the centre of rotation.

C. Wheel Movement

The movement of a wheel $\vec{v}_w(t)$ is described by a circular rotation $\vec{\omega}_w$ around the wheel hub in combination with the ego motion. In case of non slipping wheels the amount of wheel tread speed $|\vec{v}_{t,w_{tread}}(t)|$ is equal to the cyclist speed of movement. Adding $\vec{v}_{ego}$ and $\vec{v}_{t,w_{tread}}(t)$ a range of velocity occurs between zero and twice the ego motion. Each part of rim and spoke has its own speed $\vec{v}_{t,w}(t)$ depending on the distance $\vec{r}(t)$ to the wheel hub.

$$\begin{aligned} \vec{v}_{t,w}(t) &= \vec{\omega}_w \times \vec{r}(t) \\ \vec{v}_w(t) &= \vec{v}_{t,w}(t) + \vec{v}_{ego} \end{aligned} \tag{3}$$

The angular speed of pedal $\vec{\omega}_p$ and wheel $\vec{\omega}_w$ is coupled via the gear transmission ratio gtr which is in the range of 0.5 to 6.

$$\vec{\omega}_w = gtr \cdot \vec{\omega}_p \tag{4}$$

III. Cyclist Model

The used abstraction of the cyclist is not a detailed grid model but approximated with reflection points as represented in Fig. 3. The distribution of points arises from measurement observations and is focused on the exploit of μ-doppler phenomenons. The unusual high number of reflection points comes from the fact that each perspective is intended to provide an accurate picture of reality while some of the points are covered and can't be seen. The number of the points is

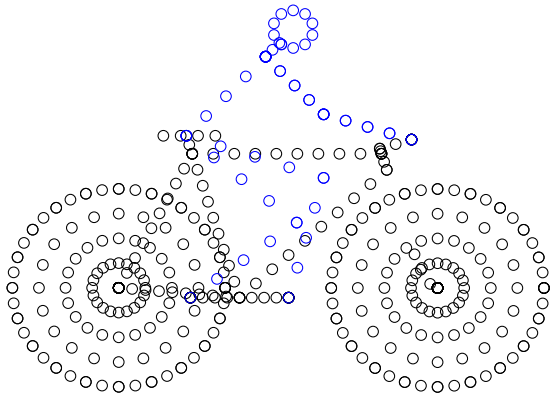

Fig. 3. Model of Cyclist represented with reflection points

variable according to different viewing angles. Another reason for this is the reflection point migration for real measurements. In fact, the reflection point moves on a target object part. To handle this and to provide radar required data, each reflection point gets several properties: position, velocity and radar cross section (RCS).

A. Point properties

1) Position: Arrangement of the points are based on measurements and fundamentals related to the technique described in [5]. The position of each model point in the simulation environment and the radar position are described by three dimensional Cartesian coordinates. Hence it is possible to get distance and direction to the radar sensor for simulation. With the direction from radar to points on the cyclist model, it is also possible to filter out points hidden or outside the visible area of the radar.

2) Velocity: Every non rotating part on the cyclist moves with the ego speed. As described in Sec. II points on rotating parts get an additional rotation dependent term. The points on the model move all in the driving direction.

3) RCS: Different measurements of the RCS from bicycles and cyclists have been shown in [6], [7]. All of them detect a dependency of the RCS value on the viewing angle. From a front view of the cyclist with ~ 0 dBsm to a view from the side with ~ -10 dBsm, the RCS value varies by around 10 dB. For simulations the visible points get an RCS value approximated by the angle of view of the whole cyclist.

B. Model dynamic

For a dynamic scenario the model has to move on a given trajectory. As input parameter, the model gets a trajectory described by direction and velocity of each part. In the particular case of bicycle models a gear transmission ratio gtr must be specified. With these parameters the exact position and velocity of each point on the cyclist model can be determined at any time.

IV. Simulator

To simulate radar data many different methods with various levels of complexity and computing effort are realizable. In the automotive area, state of the art is a chirp-sequence modulated radar system. The simulation is carried out in the baseband in order to reduce computational overhead. A detailed description of the signal generation in the baseband of a chirp-sequence radar can be found in [8], with focus on phase description. The missing information of the amplitude is approximated with the well known radar equation for point targets [9]. The radar can be placed free in orientation and position in the simulation environment. Missing input parameters like range, radial velocity and angle for each reflection point are derived from the model coordinates and the radar position. The range as absolute value of the vector between reflection points and the radar sensor is easy to identify. To estimate the radial velocity, the known speed of the reflection points is projected onto the respective range vector. The direction of arrival for the incoming signal is detectable by evaluating the differences between the RX antenna array elements.

The simulation is completely time driven. For every time step which is determined by the chirp length, the model moves, and a chirp is generated with the detected targets in view. To use the existing signal processing tool chain, the data format is customized to them.

TABLE I
Parameter of Radar and Model

Bandwidth B	Range resolution	Velocity resolution	Max. unambiguous velocity v_{max}	Cyclist v_{ego}
> 1 GHz	0.11 m	0.39 km/h	100 km/h	15 km/h

A. Simulation results

Initial simulations, with operation parameters from Tab. I, show promising results. The presented results in Fig. 4 shows a snapshot of a longitudinally moving cyclist simulated with a two dimensional antenna array. Placement of radar is behind the cyclist on the ground with view to the target (radar position $(0|0|0)$). The trajectory of the cyclist is parallel to the view of the radar in leaving direction. The gear transmission ratio has been fixed to 1.5. Target points detected with the radar are drawn in a three dimensional graph with reference position of the cyclist model at the snapshot time. The detected points of the radar compared to the reference points of the model agree with each other. The result of the range-velocity spectrum is shown in Fig. 5 (a). A representation over time is illustrated to get the ability to follow up the oscillating speed profiles on the cyclist. Looking from behind the cyclist, the influence of the pedals and rear wheel can be seen in the range-velocity spectrum. The oscillating pedal velocity around the ego motion is sticking out. It could be used as a feature to classify a cyclist over time.

V. Measurement

An important aspect in the generation of a model and the verification of the results is the comparison with real scenarios. Therefore the same scenario with the longitudinally moving cyclist is measured with a 77 GHz prototype radar as described

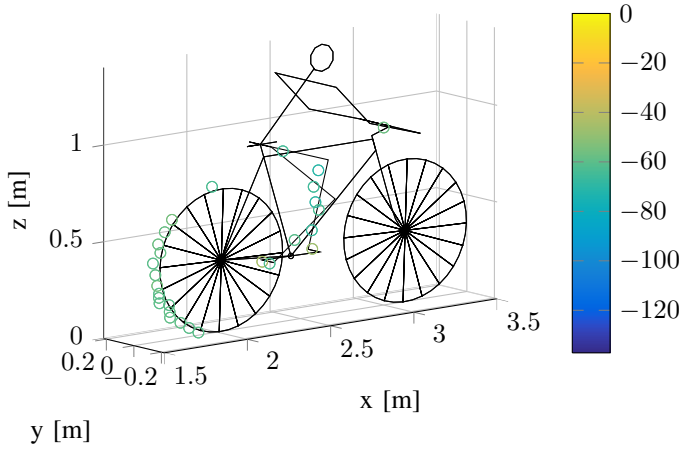

Fig. 4. 3D view of detected points from a longitudinal moving cyclist and the cyclist model as reference

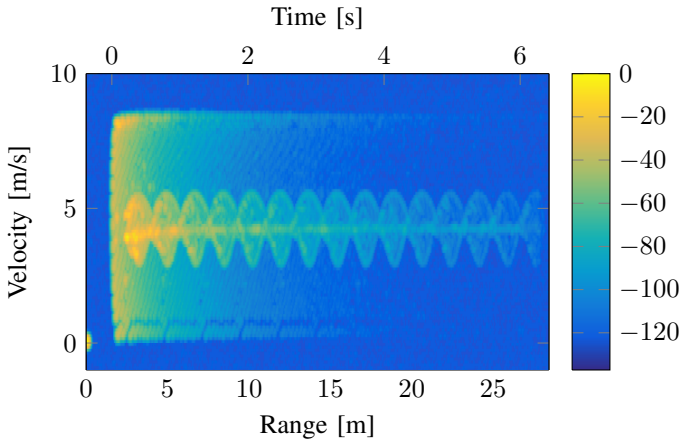

(a) Simulated data

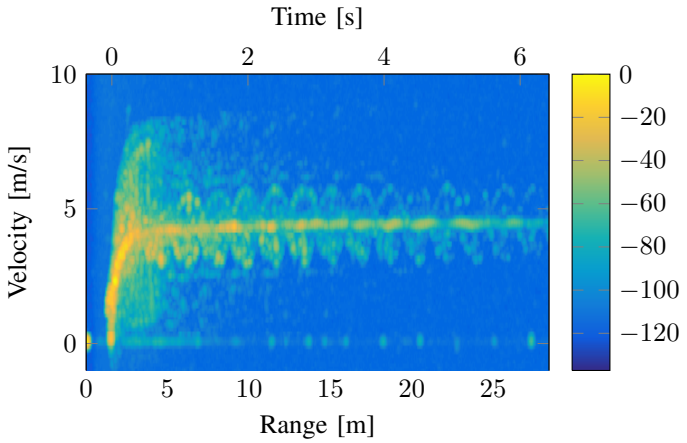

(b) Measured data

Fig. 5. Range-Velocity Spectrum of a longitudinal moving cyclist plotted over range (proportional to time)

in [10], and processed in the same way with the existing signal processing tool chain. The prototype does not provide a two-dimensional angle estimate, so only the range-velocity spectrum is compared. In Fig. 5 (b) the resulting range-velocity spectrum of the measurement data is depicted. In the near detection range, the velocity spread of the wheels can be detected. Oscillations of the pedals are detectable in the full range as shown in Fig. 5. Owing to multipath propagation and limited sensitivity of the sensor the magnitude of the signal varies.

VI. Conclusion

A way to create a model of a cyclist is presented for the simulation of radar based data. The approximation with reflection points has been described. Also the movement of a cyclist has been shown with special attention to the rotating parts legs, wheels and pedals. Results of the simulation are constituted in three dimensional Cartesian space and as range-velocity spectrum. For comparison real measured radar data with the same dynamic scenario have been recorded and processed. The match of simulation and measurement is already very good. Cyclist specific features like the rotating pedals and wheels have been observed in the data which could be used for target classification. Future work will comprise the comparison with measurement data from a two-dimensional antenna array which also enables a height estimation.

Acknowledgment

The research leading to the results of this work has received funding from the European Community's Eighth Framework Program (Horizon2020) under grant agreement n° 634149 for the PROSPECT project. The PROSPECT consortium members express their gratitude to the European Commission for selecting and supporting this project.

References

[1] E. Schubert, F. Meinl, M. Kunert, and W. Menzel, "High resolution automotive radar measurements of vulnerable road users - pedestrians & cyclists," in *Microwaves for Intelligent Mobility (ICMIM), 2015 IEEE MTT-S International Conference on*, April 2015, pp. 1–4.

[2] S. Heuel and H. Rohling, "Pedestrian recognition in automotive radar sensors," in *Radar Symposium (IRS), 2013 14th International*, vol. 2, June 2013, pp. 732–739.

[3] V. C. Chen, F. Li, S. S. Ho, and H. Wechsler, "Micro-doppler effect in radar: Phenomenon, model, and simulation study," *IEEE Transactions on Aerospace and Electronic Systems*, vol. 42, no. 1, pp. 2–21, Jan 2006.

[4] K. J. Astrom, R. E. Klein, and A. Lennartsson, "Bicycle dynamics and control: adapted bicycles for education and research," *IEEE Control Systems*, vol. 25, no. 4, pp. 26–47, Aug 2005.

[5] M. Gressmann, *Fahrradphysik und Biomechanik - Technik Formeln Gesetze*. Delius Klasing, 2010.

[6] D. Belgiovane and C. C. Chen, "Bicycles and human riders backscattering at 77 ghz for automotive radar," in *2016 10th European Conference on Antennas and Propagation (EuCAP)*, April 2016, pp. 1–5.

[7] K. Geary, J. Colburn, A. Bekaryan, S. Zeng, B. Litkouhi, and M. Murad, "Automotive radar target characterization from 22 to 29 ghz and 76 to 81 ghz," in *Radar Conference (RADAR), 2013 IEEE*, April 2013, pp. 1–6.

[8] C. Schroeder and H. Rohling, "X-band fmcw radar system with variable chirp duration," in *Radar Conference, 2010 IEEE*, May 2010, pp. 1255–1259.

[9] M. I. Skolnik, *Radar Handbook*, 2nd ed., M. I. Skolnik, Ed. McGraw Hill, 2008.

[10] F. Meinl, M. Stolz, M. Kunert, and H. Blume, "An experimental high performance radar system for highly automated driving," in *IEEE MTT-S 2017 International Conference on Microwaves for Intelligent Mobility*, 2017.